

A Simple Preparation Process of Pure $\text{Mn}_{3-x}\text{Co}_x\text{O}_4$ ($x = 1, 1.5$ and 2) Desert Rose-Like Nanoparticles and Their Optical Properties

Guillaume Salek¹, Sophie Guillemet-Fritsch¹, Pascal Dufour¹ & Christophe Tenailleau¹

¹ Institut Carnot CIRIMAT, Université Paul Sabatier, Toulouse, France

Correspondence: Christophe Tenailleau, Institut Carnot CIRIMAT, Université Paul Sabatier, 118 route de Narbonne, Toulouse 31062, France. Tel: 33-(0)561-556-293. E-mail: tenailleau@chimie.ups-tlse.fr

Received: October 24, 2012 Accepted: November 5, 2012 Online Published: November 21, 2012

doi:10.5539/ijc.v4n6p44

URL: <http://dx.doi.org/10.5539/ijc.v4n6p44>

Abstract

Monodisperse CoMn_2O_4 , $\text{Co}_{1.5}\text{Mn}_{1.5}\text{O}_4$ and Co_2MnO_4 nanoparticles were prepared by a rapid and low cost method. The organic and complex dispersing agent free synthesis of stable colloidal suspensions containing pure nanoparticles of spinel oxides was optimized at low temperature ($T < 100$ °C). The key point of the synthesis is the fast introduction of the precursor solution into a much larger volume of alkaline solution buffered with LiOH. XRD, SEM-FEG and HRTEM performed on desert rose-like nanoparticles showed that nanoparticles are crystallized and of uniform shape/size distributions. Thermogravimetric analyses give an insight into the sample composition of nanopowders in relation with semiconductor ceramic counterparts. The UV-Vis absorption spectra of these pure spinel oxide nanoparticles in solution are discussed.

Keywords: colloidal suspension, manganese and cobalt oxide, spinel; nanoparticles, UV-visible absorption

1. Introduction

Manganese and cobalt spinel oxide materials have been largely studied over the past decades thanks to their fundamental and industrial interests. The variety of oxidation states and radii for both transition metals associated with two possible polyhedral (octahedral and tetrahedral) environments can generate complex cation distributions. Thus, their structural characteristics as well as their chemical, electronic, magnetic and optical properties, often related to each other, offer many opportunities to use them for different applications such as photocatalysis (Salker & Gurav, 2000; Saadi, Bougelia, & Trari, 2006; Rios, Gautier, Poillierat, & Chartier, 1998), thermistors (Legros, Metz, & Rousset, 2006; Rousset et al., 2012), inks and pigments (Mesikova, Trojan, & Sulcova, 2005), electrochromic devices (Svegl, Orel, Hutchins, & Kalcher, 1996), photoelectrochemical decomposition of water (Walsh et al., 2009), ion-storages (Lavela, Tirado, & Vidal-Abarca, 2007), chemical sensors, and fuel cells (Xu, Wen, Wang, & Wen, 2011).

Nanoparticles can exhibit different properties than bulk material counterparts owing to their small sizes. Spinel oxide nanoparticles engineering and control is also of great interest because of their potential applications in many areas of technology including magnetic data storage, battery materials, biosensors, nanoelectronics, catalysis... The usual solid state routes can lead to the formation of mixed oxide materials but require high temperature and larger grain sizes. In order to prepare pure oxide nanoparticles with tailored morphology and size, often limited to one or a small range of composition, experimental methods usually involve a few complex stages of reaction process and organics as coordinating and/or dispersing agents. For instance, nanocrystalline spinel oxide powders and ceramics were obtained with the use of microemulsions and a sol-gel type synthesis based on the principle of controlled hydrolysis of alkoxide precursors in water droplets (Meyer, Hempelmann, Mathur, & Veith, 1999). Sun et al. (2004) prepared iron-rich cobalt or manganese spinel oxide nanoparticles by mixing iron acetates with surfactants using airless procedures. The mixture was heated up to 300 °C and hexane was used as a dispersing agent. Phenyl ether or benzyl ether were used as solvents to control the final sizes of nanoparticles. More recently, nanosized grains of cobalt and manganese spinel oxide (namely, CoMn_2O_4) were obtained by chemical co-precipitation method after decomposition of their respective metal chlorides, sodium carbonate and ethylene diamine tetra acetic acid or EDTA used as the capping agent (Tharayil, Raveendran, & Vaidyan, 2008). Nanospheres and nanorods of zinc and manganese spinel oxides, which can be used as electrode materials, were obtained by annealing an oxalate precursor and refluxing at temperature varying from 250 °C to 600 °C (Menaka, Samal, Ramanujachary, Govind, & Ganguli, 2011). Lithium manganospinel nanoparticles (30

to 300 nm) were synthesized by hydrothermal methods at 200 °C employing potassium permanganate, lithium hydroxide and acetone as synthons (Hao, Gourdon, Liddle, & Bartlett, 2012). Cheng et al. (2011) showed a simplified procedure of elaboration of nanocrystalline manganite spinels from the reduction of amorphous MnO_2 in aqueous M^{2+} solution using KMnO_4 and manganese acetate precursors. NaH_2PO_2 or NaBH_4 used as reductants and a vacuum-dried stage at 80 °C for 12 hours were required in order to form tetragonal or cubic spinels. Spinel (Zn, Co or Ni) Mn_2O_4 nanoplate assemblies were lately fabricated using the “escape-by-crafty-scheme” strategy (Zhao et al., 2012). It is explained that the formation of spherical micronic particles implies a two-step process starting from nanoscale mixed metal-organic framework precursor and organic ligands followed by thermal treatment at $T > 350$ °C. Therefore, synthetic methods used for the preparation and dispersion of spinel oxide nanoparticles can be complex and usually require the addition of organic agents.

We here report a facile synthetic route of spinel oxide nanoparticles which are very stable in colloidal suspensions. This low cost technique used to prepare pure Mn-rich and Co-rich spinel oxides with interesting solar absorbing properties could also be of a great interest for the preparation in large quantities of many other types of materials at the nanometer scale.

2. Experimental Section

2.1 Synthesis of Nanoparticles

Three compositions of cobalt-manganese oxide nanoparticles, namely CoMn_2O_4 , $\text{Co}_{1.5}\text{Mn}_{1.5}\text{O}_4$ and Co_2MnO_4 , were prepared by a simple and surfactant-free method. Cobalt (II) and manganese (II) sulfates (or nitrates) were dissolved in distilled water with the appropriate stoichiometric amounts. Solutions were voluntarily close to the saturation point in order to promote the germination before growth of nanoparticles (Marcilly, 1984). Each solution was quickly mixed in a larger volume of alkaline buffered solution ($V_{\text{salt}}/V_{\text{buffer}} = 0.7$) containing LiOH (pH~12) and left under constant stirring for 30 minutes at room temperature. The compound was then washed thoroughly with distilled water in order to remove any interfering ions. The following step consists in a reflux at 100 °C for 3 hours in the presence of a small quantity of glacial acetic acid. During the reflux stage, a complete solution of metal oxide nanoparticles was formed by providing oxygen to the alkali hydroxide precursors. Water was then replaced by absolute ethanol (used as capping agent due to a larger dipolar moment). After several washes in ethanol and a final sonication, colloidal suspensions of pure transition metal oxide nanoparticles are stabilized for 2 to 3 months.

2.2 Characterization

X-ray diffraction (XRD) data were recorded on a Bruker D4-ENDEAVOR diffractometer using $\text{CuK}\alpha$ radiation (40 kV, 40 mA) and collected over the range $10^\circ < 2\theta < 100^\circ$ at room temperature with a 0.02° step scan and 3.6 s/step.

The oxide nanoparticles were observed with a JEOL 6700F Scanning Electron Microscope (SEM) with a Field Emission Gun (FEG) and a JEOL 2100F High Resolution Transmission Electron Microscope (HRTEM) both using a 200 kV voltage. A few drops of the ethanol suspensions were placed on a glass substrate or carbon-coated Cu TEM grid, respectively.

Thermal gravimetric measurements were carried out with ~25 mg of sample using a SETARAM TAG 1750 instrument under air flow from room temperature to 1300°C (heating rate = 2.0 °C/min).

The BET (Brunauer-Emmett-Teller) specific surface areas were calculated from the nitrogen sorption experiments performed at room temperature with a Micrometrics Flowsorb II 2300.

A Zetasizer SZ90 (scattering angle of 90°) was used in order to determine the Zeta potential and agglomerate size for each solution at room temperature. Zeta potential was calculated from the electrophoretic mobility using the Henry equation of the Smoluchowski approximation (Henry, 1931). 50 μL of suspension were diluted in 5 mL of absolute ethanol before measurement. Similar Zeta potential and hydrodynamic agglomerate diameter values were obtained with different dilutions which show that the effect of a multiple scattering and the interaction between particles is negligible.

Ultra Violet-Visible-Near InfraRed (UV-Vis-NIR) absorption measurements were performed on dilute colloidal suspensions by using a Perkin Elmer Lambda 19 spectrophotometer.

3. Results and Discussion

We have achieved the rapid synthesis (within 8 hours) of pure $\text{Co}_{3-x}\text{Mn}_x\text{O}_4$ ($x = 1, 1.5, 2$) spinel oxides without any surfactant or dispersing agent but ethanol. We believe that the key point of the synthesis is the fast introduction of the close to saturation precursor solution into a much larger volume of alkaline solution buffered

with LiOH. Three representative nanocrystalline spinels were prepared and characterized. Dark colored colloidal suspensions were stabilized after synthesis. Zeta potential was measured in order to determine the potential difference between the dispersion medium and the stationary layer of fluid attached to the dispersed particle. A maximum value of +31, +29 and +26 mV was obtained for Co_2MnO_4 , $\text{Co}_{1.5}\text{Mn}_{1.5}\text{O}_4$ and CoMn_2O_4 , respectively, evidencing stability of the colloidal dispersions. The hydrodynamic agglomerate sizes are of 69 , 97 and 103 ± 6 nm, respectively (see Figure 1) with a uniform homogeneity in size distribution of particles in solutions. A scheme of agglomerate and a dark colloidal suspension of Co_2MnO_4 are shown in insets of Figure 1 to illustrate the synthetic products.

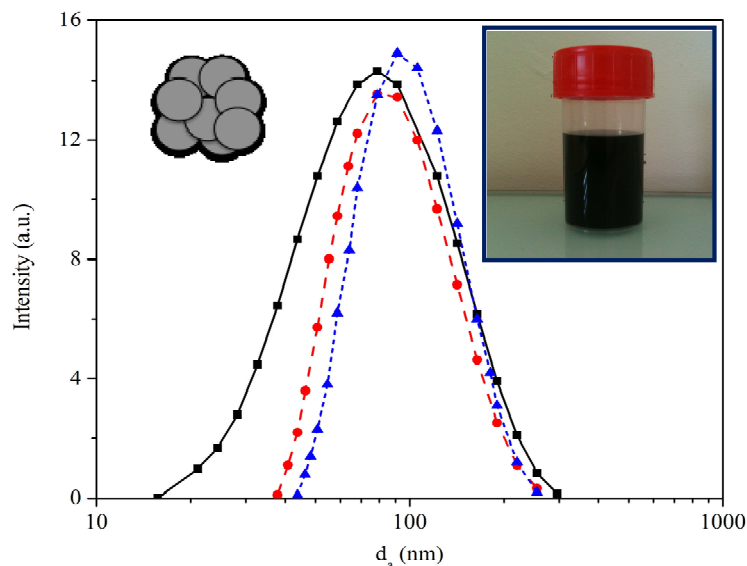


Figure 1. Hydrodynamic agglomerate (schematic in inset) size or d_a for Co_2MnO_4 (straight line and square symbols), $\text{Co}_{1.5}\text{Mn}_{1.5}\text{O}_4$ (dashes and circles) and CoMn_2O_4 (dots and triangles) colloidal suspensions. Co_2MnO_4 solution is shown in inset (suspensions of the other two compositions are visually identical)

X-ray diffraction patterns are shown in Figure 2. Co_2MnO_4 is of cubic symmetry ($Fd-3m$ space group) $\text{Co}_{1.5}\text{Mn}_{1.5}\text{O}_4$ and CoMn_2O_4 are of tetragonal symmetry ($I4_1/amd$), similarly to bulk counterparts (Bordeneuve et al., 2010a). At room temperature, it is known that $\text{Mn}_{3-x}\text{Co}_x\text{O}_4$ undergoes a symmetry transition at $x \sim 1.7$ where a peak splitting is observed for some peaks of the cubic phase as the symmetry is lowered (Aukrust & Muan, 1964). The strongest line (311) of the cubic phase is replaced by the (211) for the tetragonal phase. All compounds are pure and the peak shapes are characteristics of nanometer scale size crystallites. A crystallite size of $\sim 15(4)$ nm is determined by using Scherrer's law (and Williamson-Hall's calculation), while making the assumption of perfectly spherical particles.

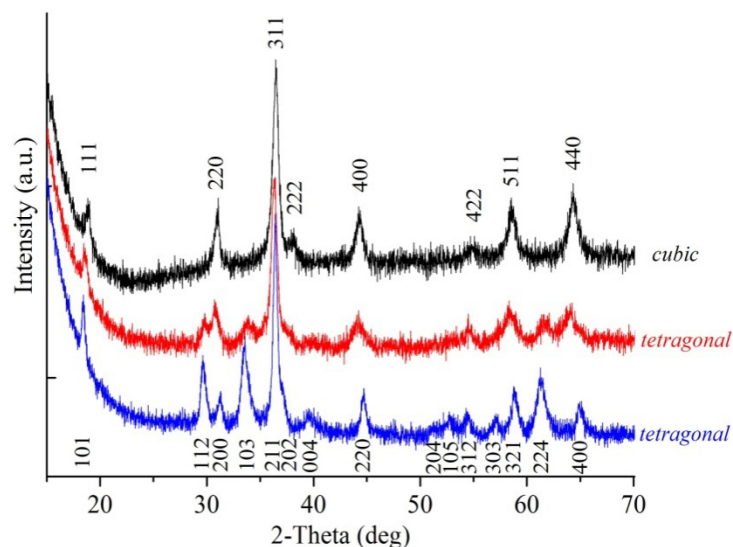


Figure 2. X-ray diffraction patterns of Co_2MnO_4 (top), $\text{Co}_{1.5}\text{Mn}_{1.5}\text{O}_4$ (middle) and CoMn_2O_4 (bottom) nanopowders. Miller indices are indicated for the cubic and tetragonal phases

FEG-SEM images show isomorph and spherical nanoparticles which look like desert-roses (Figure 3). An average nanoparticle diameter size of 23 ± 8 nm was determined by measuring for each sample the size of twenty particles observed on the SEM micrograph ($\times 10^5$). Surface areas varying from 50 to 63 ± 2 m^2/g after BET measurements confirmed this nanoparticle size of 18 ± 3 nm ($\text{diam.} = 6/S_w \cdot \rho$ where S_w is the specific surface area and ρ is the relative density). Energy Dispersive X-ray spectroscopy (EDX) spectra confirmed the stoichiometric proportions of elements in each sample (see Figure 3). HRTEM images proved that the as-prepared nanoparticles are crystallized (Figure 4). The d-spacing values of 0.29 nm between the (220) planes of the single cubic spinel phase, and 0.36 nm and 0.41 nm for the (112) and (200) planes, respectively, of the single tetragonal spinel phases, confirmed the XRD results.

The thermal gravimetric analysis (TGA) curves together with the derivatives of the TG curves (DTG) are shown in Figure 5. The DTG curve is often useful in revealing extra detail such as small events at some temperatures which are hard to be seen on the TG curve itself. It was sometimes used to determine inflection points on the TG curve, to provide reference points for weight change measurements. A first step is noticed below 200 °C, which corresponds to the loss of water and/or solvent adsorbed at the surface of the samples. This phenomenon can continue further upon heating and mix with the loss of remaining hydroxyl units. The changes observed between ~200 °C and ~400 °C can be attributed to the $\text{Mn}^{3+} = \text{Mn}^{4+}$ reaction that is favored by the nanometric state of powders (Gillot, 1994). The small gain mass in this region, also noticed by previous colleagues working on similar compositions, can be attributed to the absorption of oxygen at low annealing temperatures for the slightly under stoichiometric samples (Hao et al., 2012). A final mass loss is observed for Co_2MnO_4 and $\text{Co}_{1.5}\text{Mn}_{1.5}\text{O}_4$ starting at ~1000 °C and 1180 °C, respectively. According to our previous studies performed on ceramics of similar compositions (Bordeneuve, Rousset, Tenailleau, Guillemet-Fritsch, 2010b) this mass loss would be related to the simultaneous reduction of Co^{3+} to Co^{2+} and Mn^{4+} to Mn^{3+} . The weight losses calculated for Co-rich phases would lead to a $\text{Co}^{2+}[\text{Co}^{2+}_{0.5}\text{Co}^{3+}_{0.5}\text{Mn}^{3+}_{0.5}\text{Mn}^{4+}_{0.5}]_2\text{O}_4$ distribution for Co_2MnO_4 and $\text{Co}^{2+}[\text{Co}^{2+}_{0.25}\text{Co}^{3+}_{0.25}\text{Mn}^{3+}_{1.25}\text{Mn}^{4+}_{0.25}]_2\text{O}_4$ composition for $\text{Co}_{1.5}\text{Mn}_{1.5}\text{O}_4$. However, the reduction processes are not fully completed at the highest temperature of TGA measurements ($T = 1300$ °C) and it is not observed for CoMn_2O_4 nanopowders, in accordance with previous results obtained on ceramics (Bordeneuve et al., 2010a).

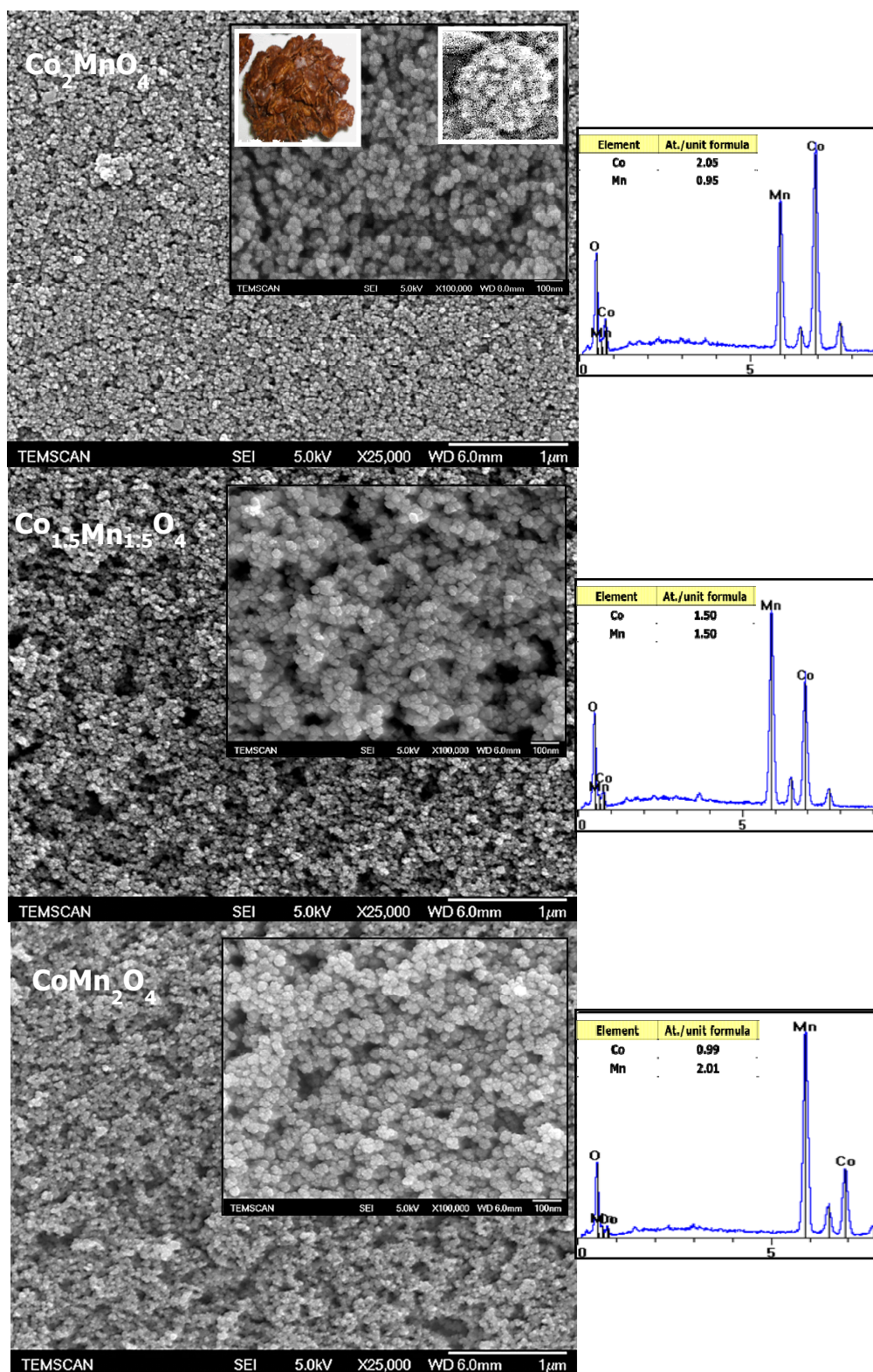


Figure 3. SEM-FEG images of $\text{Mn}_{3-x}\text{Co}_x\text{O}_4$ nanoparticles, with $x=1, 1.5$ and 2 from bottom to top. Insets are high magnifications images showing the desert-rose like shape of nanoparticles. EDX-spectra corresponding to the image analyses are given on the right (scale is in keV)

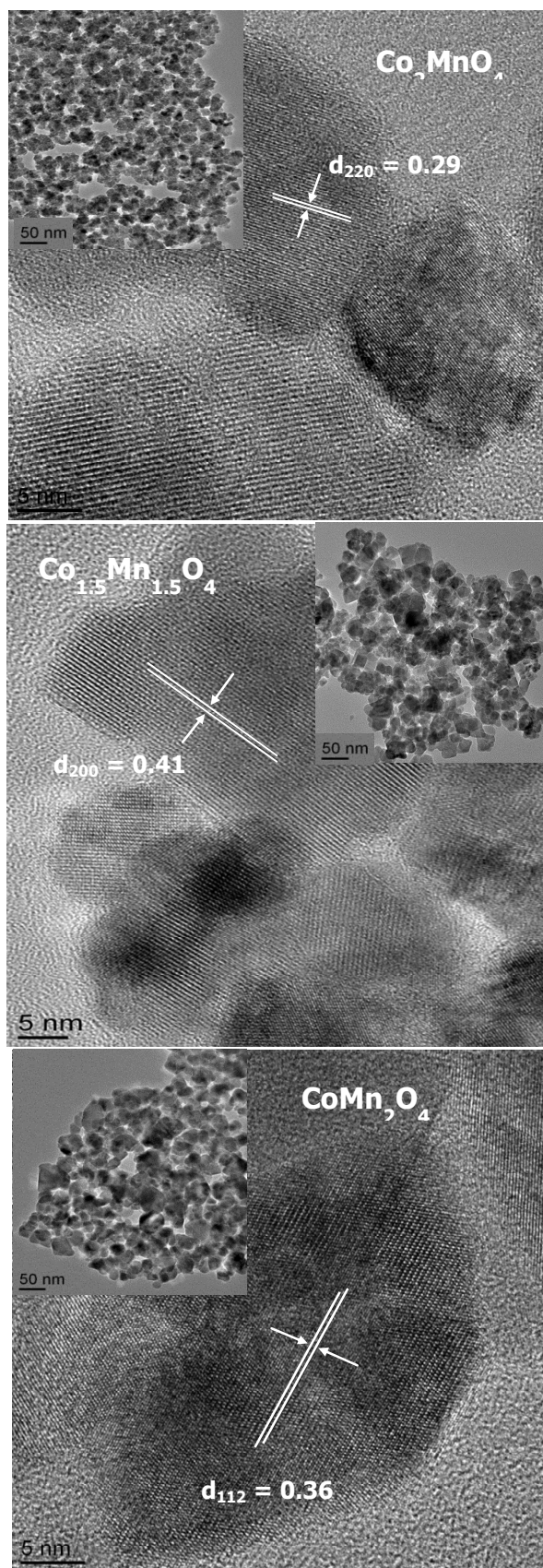


Figure 4. HRTEM images of Co_2MnO_4 (top), $\text{Co}_{1.5}\text{Mn}_{1.5}\text{O}_4$ (middle) and CoMn_2O_4 (bottom) nanoparticles; d-spacings are given in nm

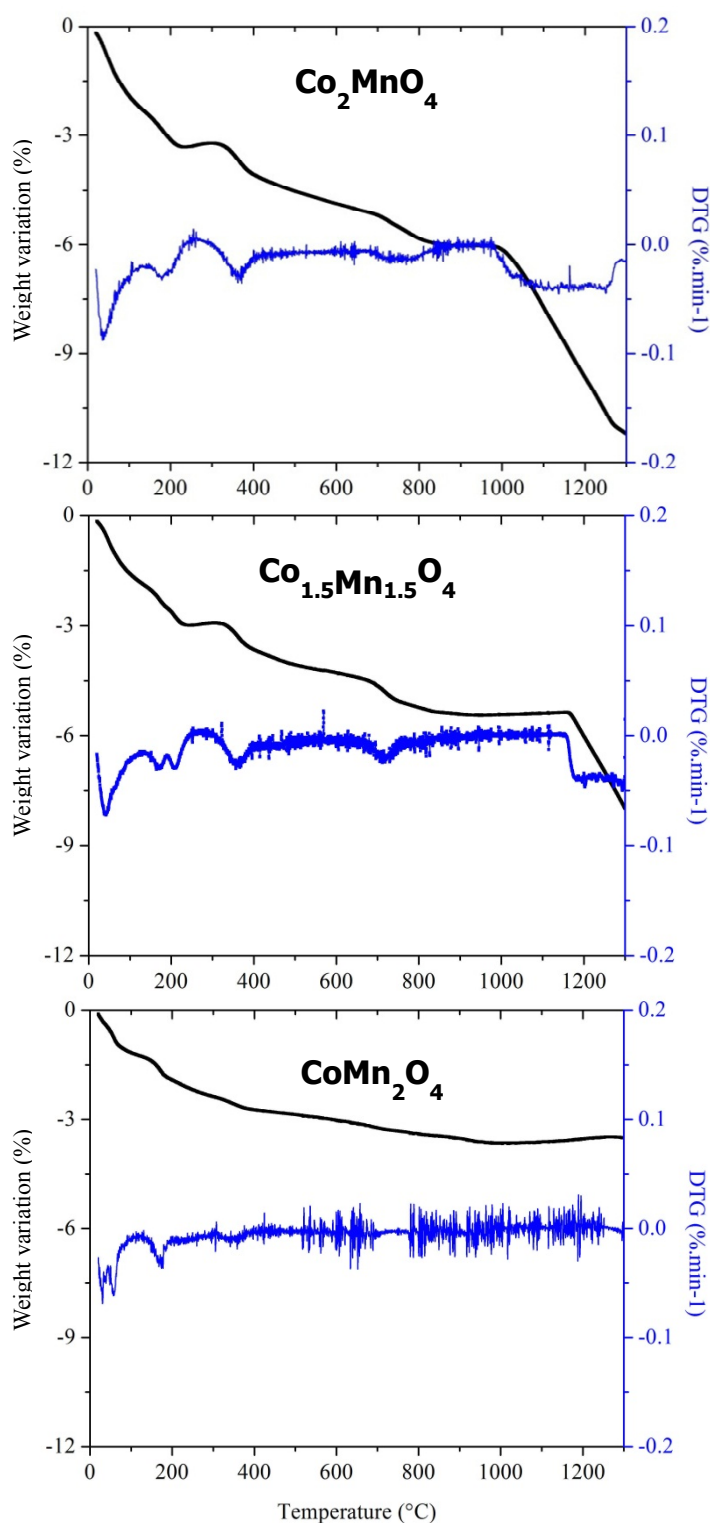


Figure 5. Thermal gravimetric analysis (TGA) and differential analysis (DTG) curves for Co_2MnO_4 (top), $\text{Co}_{1.5}\text{Mn}_{1.5}\text{O}_4$ (middle) and CoMn_2O_4 (bottom) nanopowders

The dark $\text{Co}_{3-x}\text{Mn}_x\text{O}_4$ ($x = 1, 1.5, 2$) nanoparticles display absorbance of light in the UV and early visible spectra, as shown in Figure 6. The absorbance slowly increases with the manganese content. Two absorption bands at ~ 550 nm and ~ 700 nm are observed in the visible region. Tharayil et al. (2008) attributed the first one to the

excitation of surface plasmons in the composite nanoparticles. The second change in wavelength was explained by a possible coupling of the plasmon modes between neighboring particles.

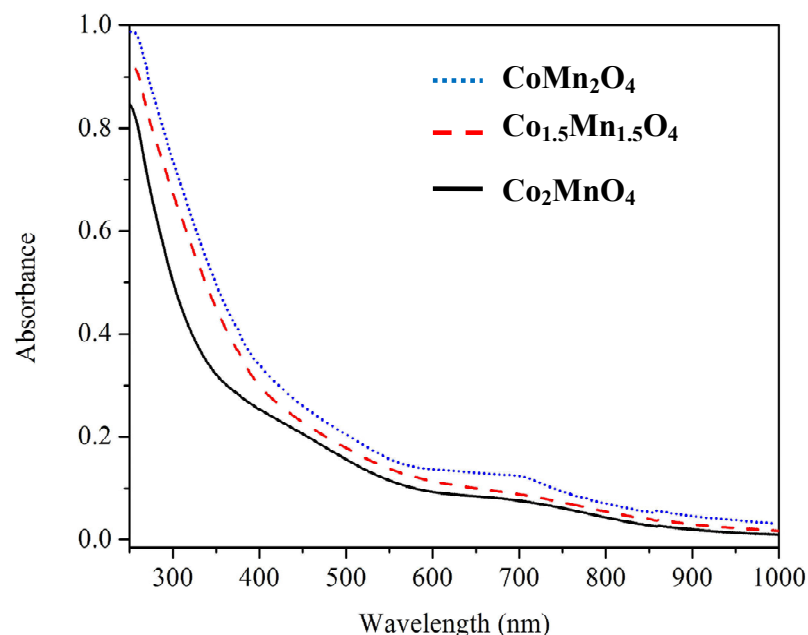


Figure 6. UV-Visible absorption spectra of CoMn_2O_4 (top), $\text{Co}_{1.5}\text{Mn}_{1.5}\text{O}_4$ (middle) and Co_2MnO_4 (bottom) nanoparticles in suspension

The optical band gap can be determined by using the Tauc relation (Tauc, 1974). No linear relation was found for indirect transitions. The extrapolation of straight line from the $(\alpha h\nu)^2 - h\nu$ curve gives direct bandgap energy values of 2.1 eV, 2.0 eV and 2.0 eV corresponding to the first absorption band at ~550 nm and 1.4 eV, 1.5 eV and 1.6 eV corresponding to the second absorption band at ~700 nm for Co_2MnO_4 , $\text{Co}_{1.5}\text{Mn}_{1.5}\text{O}_4$ and CoMn_2O_4 , respectively. Considering that Co^{2+} occupy the tetrahedral site, the octahedral site is occupied by low spin Co^{3+} when possible and high spin $\text{Mn}^{3+}/\text{Mn}^{4+}$. Taking O 2p orbital as the valence band and M energy (where M is the metal) 3d orbital as the conduction band two main electron transitions can be considered. The larger band gap energy corresponding to the lowest absorption band in the UV-Vis spectrum can be related to an energy transition from O 2p to M 3d- e_g and the smaller band gap energy to an electron jump from the O 2p to the M 3d- t_{2g} orbital. The UV-Vis light absorption may therefore be effective in generating electron/hole charge carriers. The spinel oxide nanoparticles thus obtained will accelerate the charge carrier migration rate to the surface of the sample. Photoelectrochemical reaction or photocatalytic activity, for instance, may be enhanced by the spinel oxide as prepared. Finally, the simple preparation process described here could be easily extended to many varieties of oxide materials.

4. Conclusion

Colloidal suspensions of single phase CoMn_2O_4 , $\text{Co}_{1.5}\text{Mn}_{1.5}\text{O}_4$ and Co_2MnO_4 nanoparticles were obtained by a simple and optimized soft chemistry method based on the inorganic polycondensation of metallic salts using only water and ethanol as solvents. Their microstructural and thermal stability properties were investigated. Nanocrystallites can assemble into little entities that look like desert-rose nanoparticles which are stable in solution for a few months. The study of the sample decompositions in air suggest the cation distributions observed in ceramics counterparts with two different oxidation states for the Co and Mn couples on the octahedral sites. Light absorption of nanoparticles at low wavelengths was deduced from the UV-Vis spectra showing that their optical band gap energies could also be useful for various photo-absorption activities.

Acknowledgments

The French Ministry of Education and Research is thanked for financial contribution to the PhD student salary.

References

- Aukrust, E., & Muan, A. (1964). Thermodynamic properties of solid solutions with spinel type structure. The system $\text{Co}_3\text{O}_4\text{-Mn}_3\text{O}_4$. *Transactions of the Metallurgical Society of Aime*, 230, 378-382.
- Bordeneuve, H., Rousset, A., Tenailleau, C., & Guillemet-Fritsch, S. (2010b). Cation distribution in manganese cobaltite spinels $\text{Co}_{3-x}\text{Mn}_x\text{O}_4$ ($0 \leq x \leq 1$) determined by thermal analysis. *J. Therm. Anal. Calorim.*, 101, 137-142. <http://dx.doi.org/10.1007/s10973-009-0557-7>
- Bordeneuve, H., Tenailleau, C., Guillemet-Fritsch, S., Smith, R., Suard, E., & Rousset, A. (2010a). Structural variations and cation distributions in $\text{Mn}_{3-x}\text{Co}_x\text{O}_4$ ($0 \leq x \leq 3$) dense ceramics using neutron diffraction data. *Sol. State Sc.*, 12, 379-386. <http://dx.doi.org/10.1016/j.solidstatesciences.2009.11.018>
- Cheng, F., Shen, J., Peng, B., Pan, Y., Tao, Z., & Chen, J. (2010). Rapid room-temperature synthesis of nanocrystalline spinels as oxygen reduction and evolution electrocatalysts. *Nature Chem.*, 3, 79-84. <http://dx.doi.org/10.1038/nchem.931>
- Gillot, B. (1994). DTG curves of selective oxidation of submicrometer mixed-valency spinels—Data table for the oxidation temperature of transition-metals and its relation to the cation-oxygen distance. *J. Solid State Chem.*, 113, 163-167. <http://dx.doi.org/10.1006/jssc.1994.1355>
- Hao, X., Gourdon, O., Liddle, B. J., & Bartlett, B. M. (2012). Improved electrode kinetics in lithium manganospinel nanoparticles synthesized by hydrothermal methods: identifying and eliminating oxygen vacancies. *J. Mater. Chem.*, 22, 1578-1591. <http://dx.doi.org/10.1039/c1jm15583k>
- Henry, D. C. (1931). The Cataphoresis of Suspended Particles. Part I. The Equation of Cataphoresis. *Proc. Roy. Soc. A*, 133, 106. <http://dx.doi.org/10.1098/rspa.1931.0133>
- Lavela, P., Tirado, J. L., & Vidal-Abarca, C. (2007). Sol-gel preparation of cobalt manganese mixed oxides for their use as electrode materials in lithium cells. *Electrochim. Acta*, 52, 7986-7995. <http://dx.doi.org/10.1016/j.electacta.2007.06.066>
- Legros, R., Metz, R., & Rousset, A. (1995). The Preparation, characterization and electrical properties of electroceramics made of copper-cobalt manganite spinel: $\text{Mn}_{2.6-x}\text{Co}_{0.4}\text{Cu}_x\text{O}_4$ ($0 \leq x \leq 1$). *J. Eur. Ceram. Soc.*, 15, 463-468. [http://dx.doi.org/10.1016/0955-2219\(95\)00007-H](http://dx.doi.org/10.1016/0955-2219(95)00007-H)
- Marcilly, C. (1984). Preparation of catalysts—Part 2: Depositing a metal compound on a support. Impregnation and drying. *Rev. Inst. Fra. Petrole*, 39, 189-208.
- Menaka, S. L., Samal, K. V., Ramanujachary, S. E., Govind, & Ganguli, A. K. (2011). Stabilization of Mn(IV) in nanostructured zinc manganese oxide and their facile transformation from nanospheres to nanorods. *J. Mater. Chem.*, 21, 8566-8573. <http://dx.doi.org/10.1039/c1jm10425j>
- Mesikova, Z., Trojan, M., & Sulcova, P. (2005). Conditions of synthesis of Co-Zn-Ti-Cr spinel pigment. *Ceramics Silikáty*, 49, 48-52.
- Meyer, F., Hempelmann, R., Mathur S., & Veith, M. (1999). Microemulsion mediated sol-gel synthesis of nano-scaled MAI_2O_4 (M= Co,Ni,Cu) spinels from single-source heterobimetallic alkoxide precursors. *J. Mater. Chem.*, 9, 1755-1763. <http://dx.doi.org/10.1039/a900014c>
- Rios, E., Gautier, J. L., Poillerat G., & Chartier, P. (1998). Mixed valency spinel oxides of transition metals and electrocatalysis: case of the $\text{Mn}_x\text{Co}_{3-x}\text{O}_4$ system. *Electrochim. Acta*, 44, 1491-1497. [http://dx.doi.org/10.1016/S0013-4686\(98\)00272-2](http://dx.doi.org/10.1016/S0013-4686(98)00272-2)
- Rousset, A., Tenailleau, C., Dufour, P., Bordeneuve, H., Pasquet, I., Guillemet-Fritsch, S., ... Schuurman, S. (2012). Electrical Properties of $\text{Mn}_{3-x}\text{Co}_x\text{O}_4$ ($0 \leq x \leq 3$) Ceramics: An Interesting System for Negative Temperature Coefficient Thermistors. *Int. J. Appl. Ceram. Techno.* Early View. <http://dx.doi.org/10.1111/j.1744-7402.2011.02723.x>
- Saadi, S., Bougelia, A., & Trari, M. (2006). Photoassisted hydrogen evolution over spinel CuM_2O_4 (M=Al, Cr, Mn, Fe and Co). *Renewable Energy*, 31, 2245-2256. [http://dx.doi.org/10.1016/S0013-4686\(98\)00272-2](http://dx.doi.org/10.1016/S0013-4686(98)00272-2)
- Salker, A. V., & Gurav, S. M. (2000). Electronic and catalytic studies on $\text{Co}_{1-x}\text{Cu}_x\text{Mn}_2\text{O}_4$ for CO oxidation. *J. Mat. Sc.*, 35, 4713-4719. <http://dx.doi.org/10.1023/A:1004803123577>
- Sun, S., Zeng, H., Robinson, D. B., Raoux, S., Rice, P. M., Wang, S. X., & Li, G. (2004). Monodisperse MFe_2O_4 (M=Fe,Co,Mn) nanoparticles. *J. Am. Chem. Soc.*, 126, 273-279. <http://dx.doi.org/10.1021/ja0380852>
- Svegl, F., Orel, B., Hutchins, M. G., & Kalcher, K. (1996). Structural and Spectroelectrochemical Investigations

- of Sol-Gel Derived Electrochromic Spinel Co_3O_4 Films. *J. Electrochem. Soc.*, 143, 1532-1539. <http://dx.doi.org/10.1149/1.1836675>
- Tauc, J. (1974). *Amorphous and liquid semiconductor* (p. 159). New York: Plenum. http://dx.doi.org/10.1007/978-1-4615-8705-7_4
- Tharayil, N. J., Raveendran, R., & Vaidyan, A. V. (2008). Synthesis and characterization of nanosized cobalt-manganese spinel oxide. *Ind. J. Pure Appl. Phys.*, 46, 47-53.
- Walsh, A., Ahn, K-S., Shet, S., Huda, M. N., Deutsch, T. G., Wang, H., ... Al-Jassim, M. (2009). Ternary cobalt spinel oxides for solar driven hydrogen production: Theory and experiment. *Energy Environ. Sci.*, 2, 774-782. <http://dx.doi.org/10.1039/b822903a>
- Xu, Y., Wen, Z., Wang, S., & Wen, T. (2011). Cu doped Mn-Co spinel protective coating on ferritic stainless steels for SOFC interconnect applications. *Solid State Ionics*, 192, 561-564. <http://dx.doi.org/10.1016/j.ssi.2010.05.052>
- Zhao, J., Wang, F., Su, P., Li, M., Chen, J., Yang, Q., & Li, C. (2012). Spinel ZnMn_2O_4 nanoplate assemblies fabricated via "escape-by-crafty-scheme" strategy. *J. Mater. Chem.*, 22, 13328-13333. <http://dx.doi.org/10.1039/c2jm32261g>